

The shape of Jupiter and Saturn based on atmospheric dynamics, radio occultations and gravity measurements

E. Galanti¹, Y. Kaspi¹, and T. Guillot²

¹Department of Earth and Planetary Sciences, Weizmann Institute of Science, Rehovot, Israel

²Observatoire de la Cote d'Azur, Nice, France

Key Points:

- The shapes of Jupiter and Saturn are calculated by jointly fitting their gravity and radio-occultation measurements
- Saturn's shape has a good match to the radio-occultation measurements, while Jupiter's shape does not
- The upcoming Juno radio-occultation experiment might give better constraints on the shape of Jupiter

arXiv:2305.02647v1 [astro-ph.EP] 4 May 2023

Corresponding author: Eli Galanti, eli.galanti@weizmann.ac.il

Abstract

The shape of the two gas giants, Jupiter and Saturn, is determined primarily by their rotation rate, and interior density distribution. It is also affected by their zonal winds, causing an anomaly of $O(10\text{km})$ at low latitudes. However, uncertainties in the observed cloud-level wind and the polar radius, translate to an uncertainty in the shape with the same order of magnitude. The Juno (Jupiter) and Cassini (Saturn) missions gave unprecedented accurate gravity measurements, constraining better the uncertainty in the wind structure. Using an accurate shape calculation, and a joint optimization, given both gravity and radio-occultation measurements, we calculate the possible range of dynamical height for both planets. We find that for Saturn there is an excellent match to the radio-occultation measurements, while at Jupiter such a match is not achieved. This may point to deviations from a barotropic flow, something that is to be tested with forthcoming radio-occultation measurements by Juno.

Plain Language Summary

The shape of the gaseous planets are predominantly set by the rotation rate, but are also affected by the density structure (manifested in the planet's gravity field), and the winds at the planet's outer surface. For both Jupiter and Saturn, the gravity fields have been measured to high accuracy by NASA's Juno and Cassini missions, respectively. This, together with the observed zonal winds, allows an accurate calculation of their shapes. Further constraints can be obtained from radio-occultation measurements, which give radially dependent profiles of density for specific spatial locations. Here we propose a new method for calculating the shape of the gas giants, based on an optimization of the wind latitudinal profile, decay structure, and the polar radius, given both gravity and radio-occultation measurements. We use thermal wind balance to relate the wind to the gravity measurements, and a shape model to relate the wind and polar radius to the radio-occultation measurements. We find that for Saturn there is a good match between the calculated shape and the radio-occultation measurements, while for Jupiter, no such correlation exists. We expect the new radio-occultation measurements to be performed by Juno, to help resolve the shape of Jupiter with a better accuracy.

1 Introduction

The gas giants, Jupiter and Saturn, have a shape that is close to an oblate spheroid, set mostly by the solid-body rotation rate, but is also affected by the internal density distribution, and by the zonal winds (Hubbard, 1982; Kaula, 1966). The most prominent characteristic of the shape is a difference of about 10 percent between the equatorial and polar radii (Lindal et al., 1981, 1985). While the shape of a planet with a constant density is an exact ellipsoid, the varying density inside the gas giants causes deviation in radius in the midlatitudes of around 30 km on Jupiter and 125 km on Saturn (Buccino et al., 2020). The effect of the winds on the shape, named 'dynamical height', is smaller, and was estimated to be around 4 km and 25 km at the equator of Jupiter and Saturn, respectively. However, the uncertainties associated with the observed cloud-level winds (García-Melendo et al., 2011; Tollefson et al., 2017), together with the uncertainty in the polar radius of ± 10 km (Lindal et al., 1985), are translated to uncertainty in dynamical height of the same magnitude, rendering the calculation of the dynamical height unattainable (Buccino et al., 2020). In this study we aim to disentangle this uncertainty, taking advantage of the recent gravity measurements and the better understanding the wind profiles.

Knowledge of the exact shape of the gas giants is important for several research aspects. It is used in determining the position of measurements by spacecrafts, for example, the Juno's microwave radiometer (Bolton et al., 2017; Li et al., 2017). It can be used to better constrain the rotation rate of the planets (Helled et al., 2009; Helled, 2011; Helled et al., 2015), and has an affect on the solutions of interior models (Helled & Guillot, 2013).

Knowledge of the shape is also essential in the analysis of radio-occultations (Lindal et al., 1981, 1985), which in turn are used to validate the calculated shape.

The calculated shape of the gas giants is commonly compared against radio-occultation experiments, in which the refraction by the planet’s atmosphere, is measured via a radio signal sent from a spacecraft to Earth, and then used to calculate the altitude as function of pressure (e.g., Lindal et al., 1981, 1985). Each radio occultation transect the atmosphere at a specific geographical point and provides a vertical profile of density, pressure and temperature, as function of distance from the planet center. As the measurement depends of the density, it is by definition a reflection of isopycnal surfaces, and not equipotential surfaces as in the shape calculation discussed above. Only a few radio occultations are available for the shape estimation in each planet, from the Pioneer and Voyager missions (Table 1). The uncertainty associated with the radio-occultation measurements is estimated to be around 5 km for both Jupiter and Saturn. Later missions did not result in additional measurements that could be used for the shape estimation. No Jupiter occultations were performed by Galileo, and the few published Cassini occultations measurements at Saturn did not provide the shape information. Moreover, due to the growing opacity of the atmosphere with pressure, most radio-occultation measurements ended at a pressure of around 100 mb, which is useful for some atmospheric studies, but less so for interior studies where the 1 bar level is commonly used as an upper boundary. An estimate of the radii at 1 bar from the occultations might be obtained by an extrapolation (Helled et al., 2009).

Recently, accurate measurement of the gravity field were performed for both gas giants, with the Juno mission at Jupiter (Iess et al., 2018; Durante et al., 2020), and the Grand Finale phase of the Cassini mission at Saturn (Iess et al., 2019). These measurements enabled the calculation of the wind structure at both planets, constraining both the possible variations in the cloud-level wind, and the decay of the flows with depth, setting it to around 3000 km for Jupiter (Kaspi et al., 2018), and around 9000 km for Saturn (Galanti et al., 2019). The connection between the cloud-level winds and the gravity field provides a new constraint that could potentially improve the calculation of the shape of the giant planets, as the same winds are also affecting the shape. In addition, the rotation period of Saturn, once not fully known, with estimates ranging from of 10 h 32 min 35 s (Anderson & Schubert, 2007) to 10 h 39 min 22 s (Smith et al., 1982), is now calculated from ring seismology to be around 10 h 34 min (Mankovich et al., 2019), and is also supported by Read et al. (2009) and Helled et al. (2015). These new measurements and studies enable reexamination of the Jupiter and Saturn shape beyond the approach taken in Buccino et al. (2020). First, the connection between the winds and the gravity field can potentially reduce the uncertainty from the the cloud-level wind, which was assumed there to be latitudinally independent. Second, in that study, the polar radius was not restricted to modify the dynamical height in unique latitude-independent value, which led to a large uncertainty envelope around the calculated dynamical heights (Buccino et al., 2020, Figure 1). This uncertainty could also be reduced by looking specifically on how the polar radius affects the shape derived from the occultation measurements.

In this study, we propose a new method to better constraint the shape of Jupiter and Saturn, by combining radio occultations and gravity measurements. We start by calculating the shape using the mean values of the winds and polar radii. We then explore the range of variations in the cloud-level wind allowed by the gravity measurements, and calculate its effect on the dynamical heights. Finally, we use synergistically the occultations and gravity measurements to find optimal solutions for the shape for both planets.

2 Calculating the shape of gas giants

The shape of a gaseous planet can be calculated along equipotential surfaces, based on the measured gravity harmonics, polar (or equatorial) radius, and wind profile. We follow here the notation of Lindal et al. (1985). First, the gravitational acceleration can

be calculated using

$$g_r(r, \phi) = -\frac{GM}{r^2} \left[1 - \sum_{n=2}^{\infty} (n+1) J_n \left(\frac{R_e}{r} \right)^n P_n(\sin \phi) \right] + \frac{2}{3} \omega^2 r [1 - P_2(\sin \phi)],$$

$$g_\phi(r, \phi) = -\frac{GM}{r^2} \sum_{n=2}^{\infty} J_n \left(\frac{R_e}{r} \right)^n \frac{dP_n(\sin \phi)}{d\phi} - \frac{1}{3} \omega^2 r \frac{dP_2(\sin \phi)}{d\phi},$$

where (r, ϕ) are the radius and planetocentric latitude, G is the gravitational constant, M is the planetary mass, P_n are the Legendre polynomials, J_n are the measured gravity harmonics, and R_e is the reference planetary radius, taken here as the equatorial radius in both Jupiter and Saturn, as defined in the gravity measurements (Iess et al., 2019; Durante et al., 2020). The rotation rate ω is composed from the solid body rotation ω_o and the contribution from the zonal wind, so that

$$\omega(r, \phi) = \omega_o + \frac{V_\omega}{r \cos \phi},$$

where V_ω is the cloud-level wind projected barotropically parallel to the planetary spin axis. The shape of the planet along an equipotential surface can then be defined with

$$r(\phi) = R_p - \int_{\pi/2}^{\phi} \frac{g_\phi}{g_r} r(\phi') d\phi',$$

where R_p is the polar radius for a specific pressure, defining the equipotential along which the shape is calculated. Note that the planetographic latitude is defined as $\phi + \psi$, where $\psi = \arctan(g_\phi/g_r)$.

In all previous studies (e.g., Lindal et al., 1985; Helled et al., 2009; Buccino et al., 2020), the calculation of the shape was divided into the calculation of the static body gravitational and centrifugal potential, and then a dynamical height, resulting from the cloud-level wind, was added to this latitude dependent shape, thus relying on a linearization of the problem. Here, using the derivation discussed above, we perform a direct calculation that is potentially more precise, resulting in an improvement compared to previous studies of up to 1 km in the equatorial region, for both planets. In order to calculate the effect of the winds on the shape, i.e., the dynamical height, we calculate the shape once using the full rotation rate, ω , and once using only the solid body rotation rate ω_o . The dynamical height is then derived via the subtraction of the latter from the former. Note that in both variants of the method there is a fundamental assumption that, at the pressure level where the shape is estimated, isopycnals and isobars coincide. That is accurate for the part of the shape resulting from the solid body rotation rate, but it also implies that the winds there are barotropic (having no change in the direction parallel to the planetary spin axis), at least in the atmospheric regions probed by occultations. In section 5 we will allow for wind variations that might account for baroclinicity between the 100 mb and the cloud levels.

The calculated shape can be compared against the shape derived from radio-occultation measurements (see discussion above). For most radio occultations, the deepest pressure for which the radius can be calculated is around 100 mb. Helled et al. (2009) suggested an extrapolation of the measured radius at 100 mb to a pressure of 1 bar, based on a (latitudinally independent) 48 km height difference along the vertical to the geoid. We discuss this extrapolation in Fig. 1. Values of radio-occultation radii, gravity harmonics, and polar radii are given in Table 1.

		Jupiter			Saturn		
		Measured	Gravity optimized	Gravity + occultation optimized	Measured	Gravity optimized	Gravity + occultation optimized
Gravity harmonics $\times 10^{-8}$	J_2	-	48.82	31.23	J_2	-	-741.75
	J_3	-4.50	-4.51	-4.50	J_3	5.89	3.82
	J_4	-	-4.33	-4.77	J_4	-	113.46
	J_5	-7.23	-7.91	-7.22	J_5	-22.41	-23.61
	J_6	1.00	0.23	0.99	J_6	401.44	374.88
	J_7	12.00	11.59	12.03	J_7	10.77	6.13
	J_8	3.50	4.41	3.43	J_8	-539.77	-528.23
	J_9	-11.30	-7.88	-11.17	J_9	36.91	32.16
	J_{10}	-3.00	-4.75	-3.23	J_{10}	348.44	308.44
	RMSE of fit		1.13	0.07	RMSE of fit		12.96
	100 mb radius (km)	V2N (71.8S)	67294	67302	67298	V1N (71.2S)	54948
V1N (10.1S)		71379	71390	71384	V2X (26.6S)	58913	58913
V1X (0.07N)		71539	71554	71548	P11X (9.8S)	60138	60143
P11X (19.8N)		70944	70952	70946	V1X (2.4S)	60354	60356
P10X (28N)		70415	70413	70409	V2N (30.5N)	58545	58537
P10N (60.3N)		67934	67931	67929			
RMSE of fit			9.29	5.73	RMSE of fit		4.63
R_p (km)		66896		66894	R_p (km)	54438	54437

Table 1. Values for the gravity harmonics, occultations, and polar radii at 100 mb, for the cases shown in Fig. 1 and Fig. 3. Measured values for the Jupiter (Saturn) gravity harmonics are taken from Durante et al. (2020) (Iess et al., 2019), with J_6 , J_8 , and J_{10} values shown after subtracting the contribution expected from the static interior (Guillot et al., 2018; Galanti et al., 2019, for Jupiter and Saturn, respectively). Shape values from occultations are taken from Helled et al. (2009), with the latitude indicated in brackets. For each planet, shown are solutions for a gravity only optimization, and a joint gravity and occultation optimization. Also shown are the RMSE for each type of measurement.

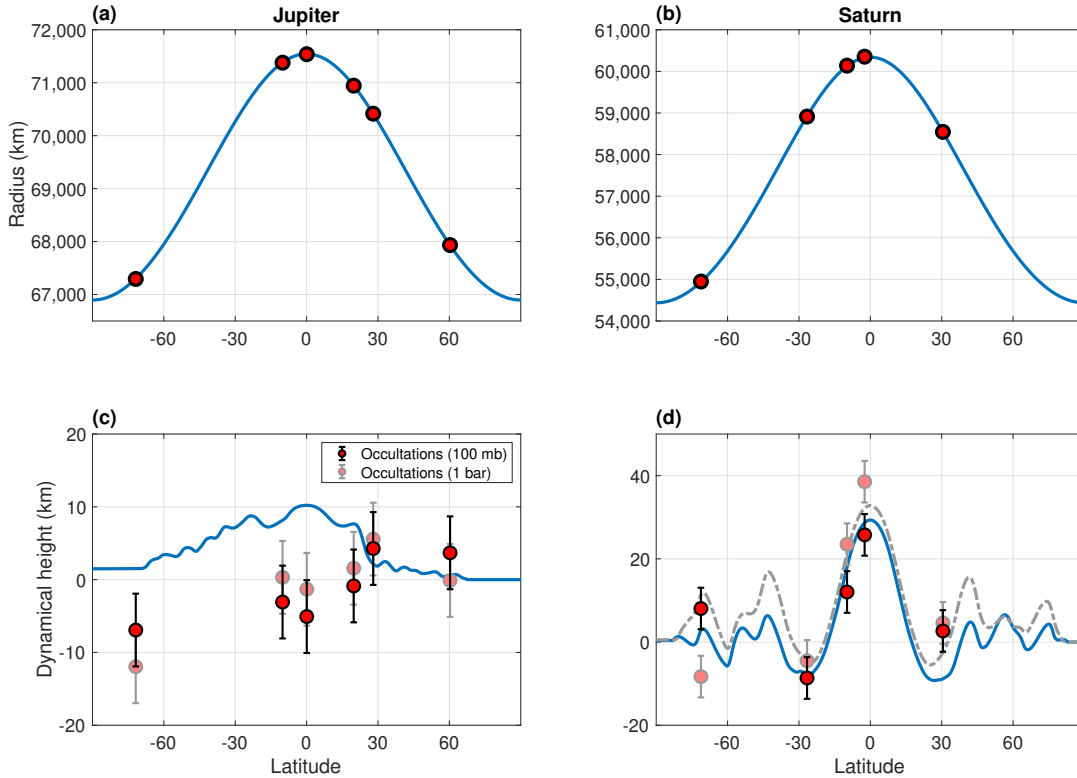


Figure 1. (a,b) the full shape of Jupiter and Saturn at 100 mb, calculated using the mean values of the measured gravity harmonics, polar radius, and wind profiles. (c,d) the dynamical height contribution (blue), taken as the difference between the shape with winds and the shape without winds, and the radii from occultation measurements at 100 mb (red dots), and 1 bar (light-red dots). For the case of Saturn, shown also is the dynamical height resulting from the gravity-based wind (dashed-gray).

3 The shape based on the observed mean values

We start with calculating the shape of the planets using the measured gravity harmonics, observed cloud-level wind, and mean value for the polar radius (Table 1). The results for the full shape at 100 mb are shown in Fig. 1, upper panels. For both planets, the overall shape is consistent with the occultations (red dots), and is similar to previous results (Lindal et al., 1981, 1985). Note that the shapes are similar to an ellipse, with differences of up to ~ 32 km for Jupiter and ~ 125 km for Saturn in the midlatitude regions (not shown). These differences result mostly from the gravity harmonics J_2 and J_4 (see Buccino et al. (2020) for a detailed analysis).

Next, we compute the dynamical height, calculated via the subtraction of the shape when calculated with a constant solid body rotation rate, from the full wind-dependent shape (Fig. 1, lower panels). The radio-occultation measurements at 100 mb are also plotted with the same solid-body shape subtracted from them as well (red dots), and we add the extrapolation of the radio occultations to 1 bar (light red dots). Since we use the same wind profile in the calculation of both the 1 bar and 100 mbar shapes, the resulting dynamical height is almost identical (with differences of a few meters). We therefore present in Fig. 1 only the dynamical height for the 100 mb level. Conversely, the radio occultations differ between the two pressure levels. This is most likely a result of an inaccurate extrapolation

of the measurements from 100 mbar to 1 bar, but might also reflect a baroclinic structure at these altitudes.

In the case of Jupiter (Fig. 1c), at both pressure levels, there is no apparent fit of the wind-induced dynamical height to that observed by the occultation measurements. The root-mean-square error (RMSE) is ~ 9 km at 100 mbar and ~ 8 km at 1 bar (Table 1), the same order of magnitude as the dynamical height itself. It seems that the difference between the dynamical height and the occultations cannot be removed by modifying the polar radius, whose uncertainty is about ± 10 km, as it will shift all occultations in the same direction, while the difference from the dynamical height is negative in the southern hemisphere and positive in the northern hemisphere. The uncertainty in the cloud-level wind has the potential to alleviate the difference. We examine these possibilities in the next sections.

In the case of Saturn (Fig. 1d), we show the dynamical heights based on two wind profiles, the observed winds (blue) and the gravity-based optimal wind structure (gray), required to fit the gravity field (Galanti et al., 2019; Militzer et al., 2019). The fit to the radio occultations is much better than in the case of Jupiter, with the dynamical height clearly following the occultation measurements. Using the optimal wind structure, the fit at the 100 mb level has an RMSE of ~ 6 km and at the 1 bar level the RMSE is ~ 4 km (Table 1). Therefore, at 100 mb, the RMSE in Saturn is about 30% smaller than that in Jupiter, while the magnitude of the dynamical height is about three times as large. Using the observed cloud-level wind, leads to a similar RMSE at the 100 mbar, however it seems that with a constant shift of the occultation values the fit should be somewhat better. Such a shift can result from a change in the polar radius. We will examine this possibility in section 5.

Note that the results for the dynamical heights for the case of Jupiter are consistent with those found in Buccino et al. (2020). Conversely, for the case of Saturn, the results are substantially different from those of the same study, but are quite similar in latitudinal shape to the profile obtained by Anderson and Schubert (2007) with a similar rotation rate.

4 The range of gravity-based wind profiles

The results discussed above depend on two parameters that are not accurately known. First, the polar radius is known to within ± 10 km (Lindal et al., 1985). Modifying the value of the polar radius would have only a minor effect on the wind-induced dynamical height, but would shift the radio-occultations values, as they are calculated with respect to the full shape of the planet. We discuss this effect in the next section. Second, the observed cloud-level winds carry uncertainties from different sources, of up to ± 50 m s⁻¹ on Saturn (García-Melendo et al., 2011) and up to ± 20 m s⁻¹ on Jupiter (Tollefson et al., 2017; Fletcher, Orton, et al., 2020). To address this uncertainty, we define in both planets an ensemble of 1000 randomly modified cloud-level winds that are at most ± 20 m s⁻¹ (based on the Jupiter wind uncertainty) different from the observed profiles, and that still ensure the explanation of all relevant gravity harmonics (Miguel et al., 2022, see also Supporting Information). Examples from these ensembles are shown in Fig. 2a,b, together with the observed cloud-level wind of Jupiter and Saturn. As we show below, for the case of Saturn, uncertainties of ± 20 m s⁻¹ are sufficient to account for the differences between the calculated dynamical height and the radio-occultation measurements.

These wind profiles are then used to calculate the range of dynamical heights that are consistent with the gravity measurements (Fig. 2c,d). The range of wind profiles translate to a maximal range of ~ 15 km for the dynamical height of Jupiter and ~ 30 km for Saturn (gray lines). There is no variance in the north pole, as the zonal wind there is zero by definition, and the maximal variations are reached around the equator, for which

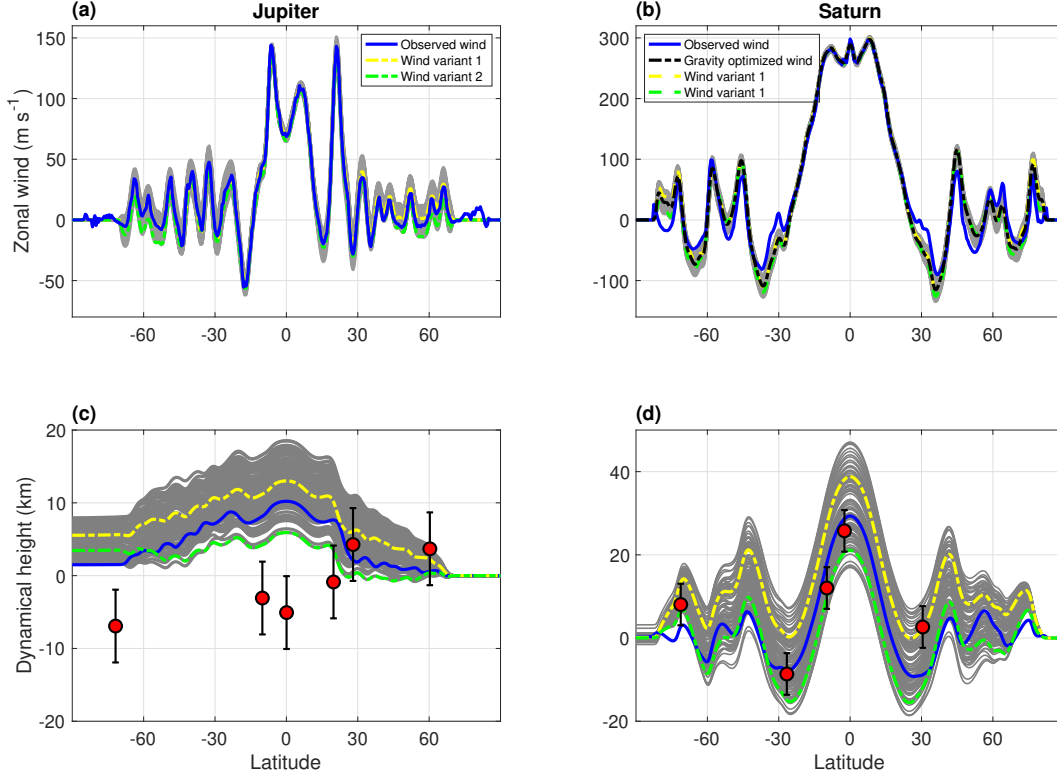


Figure 2. (a,b) the range of cloud-level wind (gray) allowing a fit to the gravity measurements. Highlighted are the observed winds (blue, (Tollefson et al., 2017) for Jupiter, and (García-Melendo et al., 2011), for Saturn) and two example variants (yellow and green). For the Saturn case, shown also is the gravity-optimized wind (dashed-black). (c,d) similar to Fig. 1, but also shown are the dynamical height resulting from the range of the wind variations (gray). Highlighted are the dynamical heights for the gravity-optimized observed wind (blue) and the two examples (yellow and green).

the dynamical height based on the observed winds is maximal. For the case of Jupiter, it is apparent that the range of the dynamical height solutions does not help to explain most of the occultations. Only the occultations at 28°N and 60.3°N are within the potential range of the dynamical heights. Conversely, for the case of Saturn, the range of dynamical heights contain all occultations.

These results illustrate the potential of fitting the wind-induced dynamical height with that indicated by the occultation measurements. While this fit seems attainable for Saturn, for Jupiter there seems little potential for finding a wind profile that would allow a fit to the occultations. This seems also the case, when considering the uncertainty in the polar radius, as it will allow only a constant shift in the occultations.

5 Wind profiles fitting the occultation measurements

Next, we aim to find specific cloud-level wind profiles, that together with a specific value for the polar radius, will explain the gravity and radio-occultation measurements. We start by calculating the optimal solution for the cloud-level wind profile (latitudinal and depth structure) and the polar radius, that allow the best fit to both the gravity field and the occultations. The latitudinal profile of the wind is allowed to deviate from its

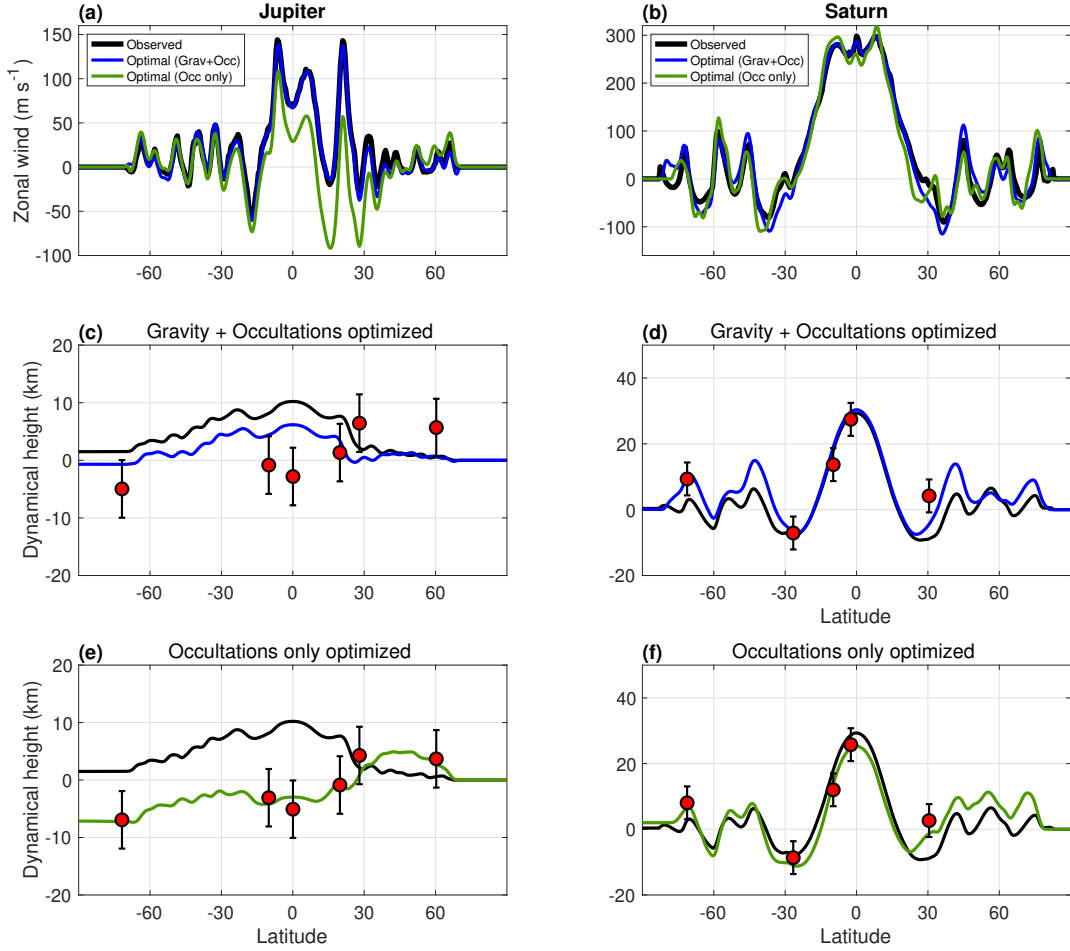


Figure 3. (a,b) the cloud-level wind, observed (black), and the optimized winds, once taking into account both gravity harmonics and occultations (blue), and the radio occultations only (green). (c,d) dynamical heights based on the observed wind (black), and the wind optimized given both gravity and occultation measurements (blue). (e,f) the same as the middle panels, but with the dynamical height based on the optimized wind given the occultation measurements only (green). Also shown are the occultation measurements (red dots). In the lower panels, the occultation values are adjusted to the optimized polar radius (see Table 1 for values).

observed value, but is kept within the observed uncertainty of around $\pm 20 \text{ m s}^{-1}$. The polar radius is allowed to vary within $\pm 10 \text{ km}$ around its mean value (Table 1). The fit to the gravity harmonics and to the occultations is examined via a cost-function set to give similar weights to both type of measurements. Finally, the optimal solutions are searched using an adjoint-based optimization procedure (see Supporting Information).

For the case of Jupiter, the optimal solution for the cloud-level wind (Fig. 3a) is quite similar to the observed wind. The dynamical height (Fig. 3c) is also quite similar, with a smaller amplitude, and the optimal polar radius is found to be smaller by 2 km than the observed mean value. The optimal dynamical height has a better fit to the occultations (Table 1), but the correlation between the latitude variations of the two data sets is still quite poor. Conversely, for the case of Saturn, with only minor changes to the gravity cloud-level wind (Fig. 3b), the dynamical height matches all 5 occultations (RMSE of 4.6 km). This confirms the analysis of the cloud-level wind range (Fig. 2).

The same methodology could be used to find the hypothetical cloud-level wind profile that allows a full fit to the occultation measurements, relaxing the restriction on the deviation of the wind from the cloud-level wind observations, and removing the requirement of fitting the gravity measurements (see Supporting information). The results are shown in Fig. 3e,f) As expected, for the case of Saturn, with only slight variations of the cloud-level wind, all radio occultations are perfectly fitted. These variations, when examined in terms of latitudinal temperature variations due to thermal wind balance, are of $O(1^\circ K)$, consistently with observations (Fletcher, Kaspi, et al., 2020). However, for the case of Jupiter, the change in the cloud-level wind (Fig. 3a, green line) is of the order of 70 m s^{-1} , much more than the observational uncertainty. Furthermore, the implied latitudinal temperature variations needed to maintain the difference between this modified wind at 100 mb and that observed at 1 bar are of $O(10^\circ K)$, based on relating the zonal wind shear to the temperature via thermal wind balance, is much higher than observed at these levels (Fletcher, Kaspi, et al., 2020).

6 Discussion and conclusion

Analyses of the shape of Jupiter and Saturn, taking into account recent understanding gained from the Juno and Cassini gravity measurements, show very different behavior between the two planets in the dynamical height exerted by the winds and that observed by radio occultations. For Saturn, we find an excellent match between the dynamical height and the occultation measurements at 100 mb. Optimizing the cloud-level wind and the polar radius, fitting both gravity and occultations measurements, results in an RMSE of 4.6 km in the fit of the dynamical height to the radio-occultation measurements, less than the uncertainty in the radio occultations. With only minor modifications of the wind profile, the radio occultation can be perfectly fitted, when excluding the gravity measurements from the optimization.

Contrary to Saturn, for Jupiter there seems to be no correlation between the calculated dynamical height and the radio occultations. No cloud-level wind profile could be found, with which the occultation measurements are matched, while satisfying the gravity constraints. Varying the polar radius does not improve that ability to match the occultations as well. One reason might be that the dynamical height in Jupiter is 3 times as small as that in Saturn, making the uncertainties in the occultation measurements more prominent. However, the result that 4 out of 6 radio-occultations measurements are completely outside the calculated dynamical height value (Fig. 3c), and have an opposite sign, suggests that something else is causing the mismatch. Fitting the radio occultation completely requires a substantially modified cloud-level wind, that is difficult to justify.

The difficulty to match the Jupiter’s calculated shape with the radio occultations can stem from two main sources. First, the radio occultation radii might be less accurate than the reported uncertainty of $\pm 5 \text{ km}$. Aside from technical issues that might have occurred during the experiments, the radio-occultation measurements depend on the knowledge of the shape itself (Lindal et al., 1981). We now know the shape of Jupiter to a better accuracy than was estimated in the days of Pioneer and Voyager, and future reanalysis of these radio occultations might potentially result in radii that are more consistent with the calculated shape. Second, it is possible that the atmosphere of Jupiter, in the range of 100 mb to 1 bar pressure levels, is baroclinic (Kaspi & Flierl, 2007), so that equipotential (pressure) surfaces are not aligned with density surfaces. We show that modifying the wind profile to fit the radio occultations requires larger latitudinal temperature variations than observed (Fletcher et al., 2021), but including departures from a barotropic flow would also require a modification of the analysis performed here. Fortunately, the Juno mission is planned to perform a multitude of radio-occultation measurements in the near future (2023-2024). These measurements, with their expected wide spatial and temporal coverage, have the potential to further constrain the shape of Jupiter, and shed light on the significance of baroclinic effects in its atmosphere.

Open Research Section

Data for the calculated shapes and radio-occultations is available via the Harvard Dataverse: <https://doi.org/10.7910/DVN/B90D83>. The rest of the data used in this study can be obtained through Helled et al. (2009), Iess et al. (2018), Guillot et al. (2018), Iess et al. (2019) and Galanti et al. (2019).

Acknowledgments

This study was supported by the Israeli Space Agency and the Helen Kimmel Center for Planetary Science at the Weizmann Institute of Science. The authors thank Prof. William B. Hubbard and an anonymous reviewer for the constructive comments.

References

- Anderson, J. D., & Schubert, G. (2007). Saturn's gravitational field, internal rotation, and interior structure. *Science*, *317*, 1384-1387. doi: 10.1126/science.1144835
- Bolton, S. J., Adriani, A., Adumitroaie, V., Allison, M., Anderson, J., Atreya, S., ... Wilson, R. (2017). Jupiter's interior and deep atmosphere: The initial pole-to-pole passes with the Juno spacecraft. *Science*, *356*, 821-825. doi: 10.1126/science.aal2108
- Buccino, D. R., Helled, R., Parisi, M., Hubbard, W. B., & Folkner, W. M. (2020). Updated Equipotential Shapes of Jupiter and Saturn Using Juno and Cassini Grand Finale Gravity Science Measurements. *J. Geophys. Res. (Planets)*, *125*(8), e06354. doi: 10.1029/2019JE006354
- Cao, H., & Stevenson, D. J. (2017). Gravity and zonal flows of giant planets: From the Euler equation to the thermal wind equation. *J. Geophys. Res. (Planets)*, *122*, 686-700. doi: 10.1002/2017JE005272
- Durante, D., Parisi, M., Serra, D., Zannoni, M., Notaro, V., Racioppa, P., ... Bolton, S. J. (2020). Jupiter's Gravity Field Halfway Through the Juno Mission. *Geophys. Res. Lett.*, *47*(4), e86572. doi: 10.1029/2019GL086572
- Fletcher, L. N., Kaspi, Y., Guillot, T., & Showman, A. P. (2020). How Well Do We Understand the Belt/Zone Circulation of Giant Planet Atmospheres? *Space Sci. Rev.*, *216*(2), 30. doi: 10.1007/s11214-019-0631-9
- Fletcher, L. N., Orton, G. S., Greathouse, T. K., Rogers, J. H., Zhang, Z., Oyafuso, F. A., ... Adriani, A. (2020). Jupiter's Equatorial Plumes and Hot Spots: Spectral Mapping from Gemini/TEXES and Juno/MWR. *J. Geophys. Res. (Planets)*, *125*(8), e06399. doi: 10.1029/2020JE006399
- Fletcher, L. N., Oyafuso, F. A., Allison, M., Ingersoll, A., Li, L., Kaspi, Y., ... Bolton, S. (2021). Jupiter's Temperate Belt/Zone Contrasts Revealed at Depth by Juno Microwave Observations. *J. Geophys. Res. (Planets)*, *126*(10), e06858. doi: 10.1029/2021JE006858
- Galanti, E., Durante, D., Finocchiaro, S., Iess, L., & Kaspi, Y. (2017). Estimating Jupiter's gravity field using Juno measurements, trajectory estimation analysis, and a flow model optimization. *Astronom. J.*, *154*(1), 2. doi: 10.3847/1538-3881/aa72db
- Galanti, E., & Kaspi, Y. (2016). An Adjoint-based Method for the Inversion of the Juno and Cassini Gravity Measurements into Wind Fields. *Astrophys. J.*, *820*(2), 91. doi: 10.3847/0004-637X/820/2/91
- Galanti, E., Kaspi, Y., Duer, K., Fletcher, L., Ingersoll, A. P., Li, C., ... Bolton, S. J. (2021). Constraints on the Latitudinal Profile of Jupiter's Deep Jets. *Geophys. Res. Lett.*, *48*(9), e92912. doi: 10.1029/2021GL092912
- Galanti, E., Kaspi, Y., Miguel, Y., Guillot, T., Durante, D., Racioppa, P., & Iess, L. (2019). Saturn's deep atmospheric flows revealed by the Cassini grand

- finale gravity measurements. *Geophys. Res. Lett.*, *46*(2), 616-624. doi: 10.1029/2018GL078087
- Galanti, E., Kaspi, Y., & Tziperman, E. (2017). A full, self-consistent treatment of thermal wind balance on oblate fluid planets. *J. Fluid Mech.*, *810*, 175-195. doi: 10.1017/jfm.2016.687
- García-Melendo, E., Pérez-Hoyos, S., Sánchez-Lavega, A., & Hueso, R. (2011). Saturn's zonal wind profile in 2004-2009 from Cassini ISS images and its long-term variability. *Icarus*, *215*(1), 62-74. doi: 10.1016/j.icarus.2011.07.005
- Guillot, T., Miguel, Y., Militzer, B., Hubbard, W. B., Kaspi, Y., Galanti, E., ... Bolton, S. J. (2018). A suppression of differential rotation in Jupiter's deep interior. *Nature*, *555*, 227-230. doi: 10.1038/nature25775
- Helled, R. (2011). Jupiter's occultation radii: Implications for its internal dynamics. *Geophys. Res. Lett.*, *38*(8), L08204. doi: 10.1029/2011GL047107
- Helled, R., Galanti, E., & Kaspi, Y. (2015). Saturn's fast spin determined from its gravitational field and oblateness. *Nature*, *520*(7546), 202-204. doi: 10.1038/nature14278
- Helled, R., & Guillot, T. (2013). Interior models of Saturn: Including the uncertainties in shape and rotation. *Astrophys. J.*, *767*, 113. doi: 10.1088/0004-637X/767/2/113
- Helled, R., Schubert, G., & Anderson, J. D. (2009). Jupiter and Saturn rotation periods. *Planet. Space Sci.*, *57*(12), 1467-1473. doi: 10.1016/j.pss.2009.07.008
- Hubbard, W. B. (1982). Effects of differential rotation on the gravitational figures of Jupiter and Saturn. *Icarus*, *52*, 509-515. doi: 10.1016/0019-1035(82)90011-2
- Iess, L., Folkner, W. M., Durante, D., Parisi, M., Kaspi, Y., Galanti, E., ... Bolton, S. J. (2018). Measurement of Jupiter's asymmetric gravity field. *Nature*, *555*, 220-222. doi: 10.1038/nature25776
- Iess, L., Militzer, B., Kaspi, Y., Nicholson, P., Durante, D., Racioppa, P., ... Zannoni, M. (2019). Measurement and implications of Saturn's gravity field and ring mass. *Science*, *364*, 1052-.
- Kaspi, Y., Davighi, J. E., Galanti, E., & Hubbard, W. B. (2016). The gravitational signature of internal flows in giant planets: comparing the thermal wind approach with barotropic potential-surface methods. *Icarus*, *276*, 170-181.
- Kaspi, Y., & Flierl, G. R. (2007). Formation of jets by baroclinic instability on gas planet atmospheres. *J. Atmos. Sci.*, *64*, 3177-3194.
- Kaspi, Y., Flierl, G. R., & Showman, A. P. (2009). The deep wind structure of the giant planets: Results from an anelastic general circulation model. *Icarus*, *202*(2), 525-542. doi: 10.1016/j.icarus.2009.03.026
- Kaspi, Y., Galanti, E., Hubbard, W. B., Stevenson, D. J., Bolton, S. J., Iess, L., ... Wahl, S. M. (2018). Jupiter's atmospheric jet streams extend thousands of kilometres deep. *Nature*, *555*, 223-226. doi: 10.1038/nature25793
- Kaspi, Y., Galanti, E., Showman, A. P., Stevenson, D. J., Guillot, T., Iess, L., & Bolton, S. J. (2020). Comparison of the Deep Atmospheric Dynamics of Jupiter and Saturn in Light of the Juno and Cassini Gravity Measurements. *Space Sci. Rev.*, *216*(5), 84. doi: 10.1007/s11214-020-00705-7
- Kaula, W. M. (1966). *Theory of satellite geodesy. Applications of satellites to geodesy.*
- Li, C., Ingersoll, A., Janssen, M., Levin, S., Bolton, S., Adumitroaie, V., ... Williamson, R. (2017). The distribution of ammonia on Jupiter from a preliminary inversion of Juno microwave radiometer data. *Geophys. Res. Lett.*, *44*(11), 5317-5325. doi: 10.1002/2017GL073159
- Lindal, G. F., Sweetnam, D. N., & Eshleman, V. R. (1985). The atmosphere of Saturn - an analysis of the Voyager radio occultation measurements. *Astrophys. J.*, *90*, 1136-1146. doi: 10.1086/113820
- Lindal, G. F., Wood, G. E., Levy, G. S., Anderson, J. D., Sweetnam, D. N., Hotz, H. B., ... Croft, T. A. (1981). The atmosphere of Jupiter - an analysis of the

- Voyager radio occultation measurements. *J. Geophys. Res.*, *86*, 8721-8727.
- Mankovich, C., Marley, M. S., Fortney, J. J., & Movshovitz, N. (2019). Cassini ring seismology as a probe of Saturn's interior. I. rigid rotation. *Astrophys. J.*, *871*, 1. doi: 10.3847/1538-4357/aaf798
- Miguel, Y., Bazot, M., Guillot, T., Howard, S., Galanti, E., Kaspi, Y., . . . Bolton, S. (2022). Jupiter's inhomogeneous envelope. *Astron. and Astrophys.*, *662*, A18. doi: 10.1051/0004-6361/202243207
- Militzer, B., Wahl, S., & Hubbard, W. B. (2019). Models of Saturn's Interior Constructed with an Accelerated Concentric Maclaurin Spheroid Method. *Astrophys. J.*, *879*, 78. doi: 10.3847/1538-4357/ab23f0
- Pedlosky, J. (1987). *Geophysical fluid dynamics*. pp. 710. Springer-Verlag.
- Read, P. L., Dowling, T. E., & Schubert, G. (2009). Saturn's rotation period from its atmospheric planetary-wave configuration. *Nature*, *460*, 608-610. doi: 10.1038/nature08194
- Smith, B. A., Soderblom, L., Batson, R., Bridges, P., Inge, J., Masursky, H., . . . Suomi, V. E. (1982). A new look at the Saturn system: The Voyager 2 images. *Science*, *215*, 505-537.
- Tollefson, J., Wong, M. H., de Pater, I., Simon, A. A., Orton, G. S., Rogers, J. H., . . . S., M. P. (2017). Changes in Jupiter's zonal wind profile preceding and during the Juno mission. *Icarus*, *296*, 163-178. doi: 10.1016/j.icarus.2017.06.007
- Zhang, K., Kong, D., & Schubert, G. (2015). Thermal-gravitational Wind Equation for the Wind-induced Gravitational Signature of Giant Gaseous Planets: Mathematical Derivation, Numerical Method, and Illustrative Solutions. *Astrophys. J.*, *806*(2), 270. doi: 10.1088/0004-637X/806/2/270